J|A|C|S ARTICLES

Published on Web 12/15/2009

Synthesis, Structure, and Bonding of Stable Complexes of Pentavalent Uranyl

Grégory Nocton,[†] Pawel Horeglad,[†] Valentina Vetere,[†,‡] Jacques Pécaut,[†] Lionel Dubois,[†] Pascale Maldivi,[†] Norman M. Edelstein,[§] and Marinella Mazzanti*[,†]

CEA, INAC, SCIB, Laboratoire de Reconnaissance Ionique et Chimie de Coordination, CEA-Grenoble, 38054 GRENOBLE, Cedex 09, France, UJF, LCIB, UMR-E 3 CEA-UJF, Grenoble I, 38041 Grenoble cedex 9, France, Université de Toulouse, Laboratoire de Chimie et Physique Quantique, UMR5626, 118 route de Narbonne, F-31062, Toulouse Cedex, France, and Lawrence Berkeley National Laboratory, Berkeley, California 94720-8175

Received May 7, 2009; E-mail: marinella.mazzanti@cea.fr

Abstract: Stable complexes of pentavalent uranyl $[UO_2(salan\text{-}^tBu_2)(py)K]_n$ (**3**), $[UO_2(salan\text{-}^tBu_2)(py)K(18C6)]$ (**4**), and $[UO_2(salophen\text{-}^tBu_2)(thf)]K(thf)_2\}_n$ (**8**) have been synthesized from the reaction of the complex $\{[UO_2py_5][KI_2py_2]\}_n$ (**1**) with the bulky amine-phenolate ligand potassium salt $K_2(salan\text{-}^tBu_2)$ or the Schiff base ligand potassium salt $K_2(salophen\text{-}^tBu_2)$ in pyridine. They were characterized by NMR, IR, elemental analysis, single crystal X-ray diffraction, UV−vis spectroscopy, cyclic voltammetry, low-temperature EPR, and variable-temperature magnetic susceptibility. X-ray diffraction shows that **3** and **8** are polymeric and **4** is monomeric. Crystals of the monomeric complex $[U^VO_2(salan\text{-}^tBu_2)(py)][Cp^*_2Co]$, **6**, were also isolated from the reduction of $[U^{VI}O_2(salan\text{-}^tBu_2)(py)]$, **5**, with Cp^*_2Co. Addition of crown ether to **1** afforded the highly soluble pyridine stable species $[UO_2py_5]I.py$ (**2**). The measured redox potentials $E_{1/2}$ (U^{VI}/U^V) are significantly different for **2** (−0.91 and −0.46 V) in comparison with **3**, **4**, **5**, **7** and **9** (in the range −1.65 to −1.82 V). Temperature-dependent magnetic susceptibility data are reported for **4** and **7** and give μ_{eff} of 2.20 and 2.23 μ_B at 300 K respectively, which is compared with a μ_{eff} of 2.6(1) μ_B (300 K) for **2**. Complexes **1** and **2** are EPR silent (4 K) while a rhombic EPR signal ($g_x = 1.98$; $g_y = 1.25$; $g_z = 0.74$ (at 4 K) was measured for **4**. The magnetic and the EPR data can be qualitatively analyzed with a simple crystal field model where the f electron has a nonbonding character. However, the temperature dependence of the magnetic susceptibility data suggests that one or more excited states are relatively low-lying. DFT studies show unambiguously the presence of a significant covalent contribution to the metal−ligand interaction in these complexes leading to a significant lowering of the π_u^*. The presence of a back-bonding interaction is likely to play a role in the observed solution stability of the $[UO_2(salan\text{-}^tBu_2)(py)K]$ and $[UO_2(salophen\text{-}^tBu_2)(py)K]$ complexes with respect to disproportionation and hydrolysis.

Introduction

Molecular uranium chemistry has undergone significant expansion in the last few decades.[1−5] One of the most exciting recent new entries into this area is pentavalent uranyl. Due to their low stability, compounds of pentavalent uranyl remain rare and only in the past few years have some isolable systems been reported. An overview of the synthesis and characterization of these systems has been recently covered in two review articles.[6,7] So far, the reactivity of the few isolated compounds in this class remain almost unexplored.[7] Aside from its high fundamental interest, the chemistry of pentavalent uranyl has important environmental implications. Notably, the UO_2^+ species has been identified as a key intermediate in the anaerobic bacterial[8,9] or mineral mediated[10] reduction of highly soluble hexavalent uranyl species to insoluble U(IV) compounds. Since this process reduces the mobility of uranium in the environment, it is highly relevant for the speciation of uranium in the environment and for the development of remediation strategies.[11] Accordingly, a better knowledge of the chemical properties of UO_2^+ will certainly contribute to the general understanding of the biogeochemical reduction of uranium in the environment. Moreover, UO_2^+ provides a reasonable and practical model for the more highly radioactive NpO_2^+ cation due to their identical

[†] CEA-Grenoble and CEA-UJF.
[‡] Université de Toulouse.
[§] Lawrence Berkeley National Laboratory.

(1) Bart, S. C.; Meyer, K. *Organomet. Coord. Chem. Actinides* **2008**, *127*, 119–176.
(2) Fox, A. R.; Bart, S. C.; Meyer, K.; Cummins, C. C. *Nature* **2008**, *455*, 341–349.
(3) Sessler, J. L.; Melfi, P. J.; Pantos, G. D. *Coord. Chem. Rev.* **2006**, *250*, 816–843.
(4) Korobkov, I.; Sandro, G. *Prog. Inorg. Chem.* **2005**, *54*, 321–349.
(5) Ephritikhine, M. *Dalton Trans.* **2006**, 2501–2516.
(6) Graves, C. R.; Kiplinger, J. L. *Chem. Commun.* **2009**, 3831–3853.
(7) Arnold, P. L.; Love, J. B.; Patel, D. *Coord. Chem. Rev.* **2009**, *253*, 1973–1978. Mougel, V.; Horeglad, P.; Nocton, G.; Pécaut, J.; Mazzanti, M. *Angew. Chem., Int. Ed.* **2009**, *48*, 8477–8480.
(8) Lovley, D. R.; Phillips, E. J. P.; Gorby, Y. A.; Landa, E. R. *Nature* **1991**, *350*, 413–416.
(9) Renshaw, J. C.; Butchins, L. J. C.; Livens, F. R.; May, I.; Charnock, J. M.; Lloyd, J. R. *Environ. Sci. Technol.* **2005**, *39*, 5657–5660.
(10) Ilton, E. S.; Haiduc, A.; Cahill, C. L.; Felmy, A. R. *Inorg. Chem.* **2005**, *44*, 2986–2988.
(11) Morris, D. E. *Inorg. Chem.* **2002**, *41*, 3542–3547.

charge. The low charge of the NpO_2^+ renders problematic its separation in nuclear fuel reprocessing.[12] The design of suitable ligands for the selective complexation and extraction of AnO_2^+ species requires a better understanding of the molecular parameters governing the bonding and reactivity of these species.

Though kinetic studies on aqueous UO_2^+ go a long way back,[13,14] the low stability of this species in aqueous solutions has prevented the isolation of UO_2^+ compounds. Pentavalent uranyl can be stabilized in concentrated carbonate media,[15−17] but otherwise it readily disproportionates to U(IV) and uranyl(VI) species.[12] Only the use of anhydrous and anaerobic conditions allowed the electrochemical production of pure UO_2^+ complexes in solution with Schiff base or diketonate ligands, but these complexes were never isolated using this route.[12,18−20] After a first report of the crystal structure of a serendipitously obtained cationic complex ($[UO_2(OPPh_3)_4]^+$),[21] only in the last three years have several complexes of pentavalent uranyl been reproducibly synthesized using different synthetic procedures.[22−31] However, most of these complexes show a limited solution stability and undergo disproportionation which is likely to involve the formation of a dimeric complex through the mutual binding of two uranyl(V) groups (commonly known as cation−cation interaction).[32] Our group has reported the only example of such intermediates, which demonstrated a sufficient stability to allow their isolation.[28] Full stability of pentavalent uranyl complexes with respect to disproportionation in solution has been obtained by Arnold and co-workers[27] in tetrahydrofuran solution, in the presence of a transition metal cation by using bulky macrocyclic ligands which disfavors dimer formation. Aside from this system, a remarkable solution stability has also been observed for the simple pyridine solvate $\{[UO_2py_5][KI_2py_2]\}_n$ (**1**)[22] and analogous complexes containing the $[UO_2py_5]^+$ unit, in spite of the absence of bulky ligands that can provide steric protection along the equatorial plane.[29] Moreover, in these complexes, the high Lewis basicity of the uranyl oxygen often results in the presence of cations coordinated to the UO_2^+ group. The little experimental information available on the reported uranyl(V) compounds suggests that electronic factors and cation binding should play an important role in the stabilization of pentavalent uranyl. We have recently shown in a preliminary communication that tetradentate bulky amine-phenolate ligands can stabilize pentavalent uranyl in pyridine solution and allows the synthesis of the stable $[UO_2(salan\text{-}^tBu_2)(py)K]_n$ polymer (Scheme 1).[30] Here we report the synthesis and structure of a new highly stable complex of pentavalent uranyl supported by the bulky Schiff base ligand salophen-$^tBu_2^{2-}$.

Scheme 1. Reaction of **1** with K_2(salan-^{t}Bu$_2$) and K_2(salophen-^{t}Bu$_2$)

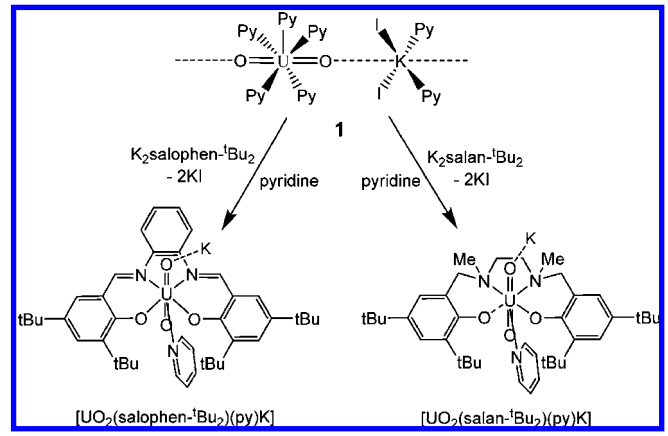

These complexes were synthesized from the previously reported iodide derivative $\{[UO_2py_5][KI_2py_2]\}_n$ (**1**)[22] according to Scheme 1. The synthesis and structure of mononuclear analogues of the salan-^{t}Bu$_2$ complex will also be described. The structural, magnetic, redox and spectroscopic properties, and the solution stability with respect to disproportionation and ligand dissociation of these complexes, have been investigated in detail. The experimental study has been paired with a qualitative analysis of the magnetic data and DFT studies of the electronic structure and bonding. The presented results provide important new information on the molecular parameters allowing the stabilization of pentavalent uranyl species, which include cation binding and steric and electronic ligand effects.

Results and Discussion

Synthesis, Molecular Structure and Reactivity. The pentavalent uranyl iodide $\{[UO_2py_5][KI_2py_2]\}_n$ (**1**), previously reported,[22] is stable in pyridine where it is however only slightly soluble. Although its solubility is sufficient for coordination chemistry studies,[28,30] its low solubility prevents the study of its solution properties. The reaction of **1** with the K_2salan-^{t}Bu$_2$ (H_2salan-^{t}Bu$_2$ = *N*,*N*′-bis(2-hydroxybenzyl-3,5-di-*tert*-butyl)-1,2-dimethylaminomethane) in pyridine led to the isolation of the stable complex $[UO_2(salan\text{-}^tBu_2)(py)K]_n$ (**3**). We have recently communicated the crystal structure of this complex.[30] The presence of $K^+\cdots UO_2^+$ cation−cation interactions in complexes **1** and **3** results in the formation of polymeric structures. Only a few mononuclear compounds of pentavalent uranyl have been reported, and all have been prepared from the reduction of the hexavalent analogue.[25,26,29] Here we show that the mononuclear compounds **2** and **4** can be isolated by reacting the polymeric complexes **1** and **3** with 18C6 (Scheme 2). 18C6 has a strong affinity for the potassium cation, and the resulting $(K18C6)^+$ complex is expected to bind less strongly to the uranyl oxygen.

(12) Morss, L. R.; Edelstein, N. M.; Fuger, J. *The Chemistry of the Actinide and Transactinide Elements*; Springer: Dordrecht, 2006.
(13) Newton, T. W.; Baker, F. B. *Inorg. Chem.* **1965**, *4*, 1166–1170.
(14) Ekstrom, A. *Inorg. Chem.* **1974**, *13*, 2237–2241.
(15) Ikeda, A.; Hennig, C.; Tsushima, S.; Takao, K.; Ikeda, Y.; Scheinost, A. C.; Bernhard, G. *Inorg. Chem.* **2007**, *46*, 4212–4219.
(16) Docrat, T. I.; Mosselmans, J. F. W.; Charnock, J. M.; Whiteley, M. W.; Collison, D.; Livens, F. R.; Jones, C.; Edmiston, M. J. *Inorg. Chem.* **1999**, *38*, 1879–1882.
(17) Clark, D. L.; Hobart, D. E.; Neu, M. P. *Chem. Rev.* **1995**, *95*, 25–48.
(18) Mizuoka, K.; Tsushima, S.; Hasegawa, M.; Hoshi, T.; Ikeda, Y. *Inorg. Chem.* **2005**, *44*, 6211–6218.
(19) Mizuoka, K.; Ikeda, Y. *Radiochim. Acta* **2004**, *92*, 631–635.
(20) Kim, S. Y.; Tomiyasu, H.; Ikeda, Y. *J. Nucl. Sci. Technol.* **2002**, *39*, 160–165.
(21) Berthet, J.-C.; Nierlich, M.; Ephritikhine, M. *Angew. Chem., Int. Ed.* **2003**, *42*, 1952–1954.
(22) Natrajan, L.; Burdet, F.; Pecaut, J.; Mazzanti, M. *J. Am. Chem. Soc.* **2006**, *128*, 7152–7153.
(23) Burdet, F.; Pecaut, J.; Mazzanti, M. *J. Am. Chem. Soc.* **2006**, *128*, 16512–16513.
(24) Berthet, J. C.; Siffredi, G.; Thuery, P.; Ephritikhine, M. *Chem. Commun.* **2006**, 3184–3186.
(25) Hayton, T. W.; Wu, G. *J. Am. Chem. Soc.* **2008**, *130*, 2005–2014.
(26) Hayton, T. W.; Wu, G. *Inorg. Chem.* **2008**, *47*, 7415–7423.
(27) Arnold, P. L.; Patel, D.; Wilson, C.; Love, J. B. *Nature* **2008**, *451*, 315–318.
(28) Nocton, G.; Horeglad, P.; Pecaut, J.; Mazzanti, M. *J. Am. Chem. Soc.* **2008**, *130*, 16633–16645.
(29) Berthet, J. C.; Siffredi, G.; Thuery, P.; Ephritikhine, M. *Dalton Trans.* **2009**, 3478–3494.
(30) Horeglad, P.; Nocton, G.; Filinchuck, Y.; Pécaut, J.; Mazzanti, M. *Chem. Commun.* **2009**, 1843–1845.
(31) Hayton, T. W.; Wu, G. *Inorg. Chem.* **2009**, *48*, 3065–3072.
(32) Steele, H.; Taylor, R. J. *Inorg. Chem.* **2007**, *46*, 6311–6318.

Scheme 2. Reaction of **1** and **3** with 18C6 Crown Ether in Pyridine

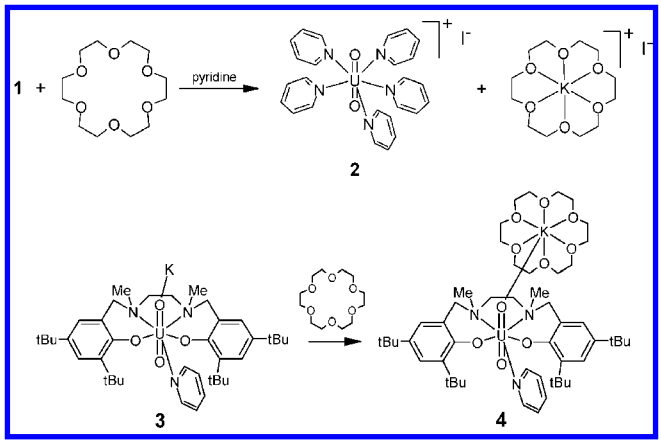

Previous studies show that the addition of 18C6 to a potassium bound tetrameric complex of pentavalent uranyl results in the disruption of the polynuclear structure.[33]

The addition of 18C6 to a suspension of **1** in pyridine leads to the complete dissolution of the complex. The stability of a 1:1 solution of **1** and 18C6 in pyridine was investigated by UV−visible spectroscopy over a period of one month, and no decomposition was observed. This result confirms the remarkable effect of the pyridine ligand in stabilizing the UO_2^+ even in the absence of coordinated cation. X-ray quality crystals of the complex $[UO_2py_5]I.py$ (**2**) were isolated by slow diffusion of hexane into a pyridine solution containing complex **1** and crown ether in a U:18C6 1:1 ratio. The molecular structure of the complex was confirmed by X-ray diffraction, which shows the presence of isolated $[UO_2(Py)_5]^+$ cation and I^- anion. During the preparation of this manuscript, crystals of complex **2** have also been obtained by reduction of the hexavalent iodide $[UO_2py_5I_2]$ with TlC_5H_5 and the crystal structure of **2** has been reported.[29]

The X-ray diffraction studies of the mononuclear complex $[UO_2(salan\text{-}^tBu_2)(py)K(18C6)]$ (**4**) show that a $K^+\cdots UO_2^+$ interaction is still present for one uranyl oxygen but does not lead to the formation of a polymeric structure. This is probably the result of the steric crowding and the lower coordinating power of the $K(18C6)^+$. To investigate the effect of the coordinating cation on the stability and redox properties of the uranyl complex, we have also used a different synthetic approach to the preparation of pentavalent uranyl that involves the reduction of the hexavalent analogue by an appropriate reducing agent. The reduction of $[UO_2(salan\text{-}^tBu_2)(py)]$ (**5**) with an excess of Cp^*_2Co led to the isolation of X-ray quality crystals of the pentavalent complex $[UO_2(salan\text{-}^tBu_2)(py)][Cp^*_2Co]$ (**6**) (Scheme 3).

However, this synthetic method does not allow the quantitative isolation of the pentavalent complex in a pure form because of the difficulty in separating the excess of cobaltocene necessary for the completeness of the reduction. The addition of potassium iodide to a solution of **6** in pyridine affords complex **3**, confirming the presence of pentavalent uranyl.

The crystal structures of complexes **4** and **6** were determined by X-ray diffraction studies. ORTEP views of **4** and **6** are presented in Figures 1 and 2, respectively, while selected bond distances and angles for **3**, **4** and **6** are given in Table 1.

(33) Nocton, G.; Horeglad, P.; Pécaut, J.; Mazzanti, M. *J. Am. Chem. Soc.* **2008**, *130*, 16633–16645.

In compounds **3**, **4** and **6**, the uranium atom is seven coordinated with regular pentagonal bipyramidal coordination geometry. The four donor atoms of the salan-$^tBu_2^{2-}$ (O_2N_2) and the nitrogen of coordinated pyridine form a pentagonal plane (with a mean deviation of 0.07 Å in **3**, 0.10 Å in **4** and 0.16 Å´ in **6**). The ligand wraps around the metal with the two methyl groups in a trans position taking a chiral pseudo-C_2 symmetry for all three complexes. Both enantiomers are found in the structure leading to a racemic space group. The axial positions are occupied by two oxo ligands with U═O distances between 1.819 and 1.868 Å (mean U═O = 1.825(8) Å for **3**, 1.859(11) Å for **4** and 1.856(14) Å for **6**), which all show a significant lengthening of the U═O bonds in comparison with the corresponding UO_2^{2+} complex $[UO_2(salan\text{-}^tBu_2)(py)]$ (U═O = 1.764(4) and 1.790(3) Å).[30] The angle O−U−O in the UO_2^+ is in the range 177.38−178.9°. The equatorial positions are occupied by the two oxygen atoms (mean U−O distance: 2.35(4) Å in **3**, 2.339(10) Å in **4** and 2.380(12) Å in **6**) and the two nitrogen atoms (mean U−N: 2.703(18) Å in **3**, 2.705(11) Å in **4** and 2.772(12) Å in **6**) of salan-$^tBu_2^{2-}$ ligand, and the nitrogen atom of the pyridine ($U-N_{pyridine}$ 2.618(16) Å in **3**, 2.629(3) Å in **4** and 2.700(11) Å in **6**). A significant lengthening of the U═O bond distances is found in **4** and **6** with respect to **3**. Surprisingly longer U═O bond distances are found in the presence of the weakly coordinating $(K18C6)^+$ cation or in absence of coordinating cation. This is associated, at least in **6** with a significant lengthening of the distance U-salan-$^tBu_2^{2-}$, suggesting that the absence of coordinated potassium has a significant effect on the interaction of the uranyl group with the ligands in the equatorial plane (see computational and magnetic data). In all of the compounds, the $U-N_{pyridine}$ distance is shorter than the $U-N_{salan}$ distances with differences ranging from 0.076 to 0.085 Å.[30] The proton NMR spectrum of pyridine solution of **3**, **4** and **6** are very similar and all show the presence of two sets of signals. One set of signals (major species) was assigned to the presence in solution of monomeric rigid C_2 symmetric enantiomers (λ and δ), consistent with the ligand conformation in the solid state structure, while the second set of signals indicate the presence of a minor C_s symmetric isomer (see Figure S1 in Supporting Information). The ratios of C_2:C_s at room temperature vary only slightly for the three complexes (from 100:6 for **3**,[30] to 100:9 for **4** and 100:14 for **6**). The ratio of C_2:C_s is temperature dependent (100:11 for **3** at 333 K),[30] suggesting the presence of an equilibrium among the different conformers in solution. All three salan-$^tBu_2$ complexes **3**, **4** and **6** show the same high stability with respect to the disproportionation reaction in pyridine and dmso solution (up to 30 days). However, a lower stability is observed for complex **3** compared to **4** in thf with partial disproportionation occurring for **3** already after 14 days (only 33% of pentavalent uranyl remaining) and full stability of **4** up to 30 days. Partial decomposition was observed also for complex **4** in toluene (only 67% of the pentavalent uranyl complex is left after 14 days).

To prepare complexes of pentavalent uranyl with increased stability toward disproportionation in all organic solvent and with higher stability toward ligand dissociation in the presence of water, we have turned to Schiff base ligands.

The formation of a $[UO_2(salophen)(dmso)]^-$ (H_2salophen = *N*,*N*′-phenylene-bis-salicylideneimine complex by electrochemical reduction of the hexavalent analogue in dmso had been

Scheme 3

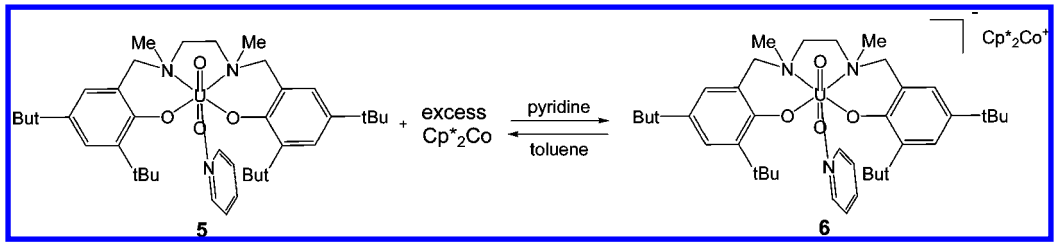

previously reported,[34] but the complex had never been isolated following this route. Our attempts to isolate the [U(salophen-)(py)K] complex from the reaction of **1** with salophen^{2-} in pyridine led to the formation of a mixture of UO_2^+, UO_2^{2+} and U(IV) products as a result of the very rapid decomposition of the pentavalent uranyl complex. To synthesize and characterize stable uranyl(V) complexes with a Schiff base ligand, we decided to investigate the reaction of **1** with the bulky Schiff base ligand salophen-^{t}Bu$_2^{2-}$ (H_2salophen-^{t}Bu$_2$ = *N*,*N*′-phenylene-bis-(3,5-di-*tert*-butylsalicylideneimine). The use of the bulkier ligand salophen-^{t}Bu$_2^{2-}$ affords the complex [UO_2(salophen-^{t}Bu$_2$)(py)K] (**7**), which shows a full solution stability (up to one month) in pyridine (Scheme 4).

The proton NMR of complex **7** in pyridine solution shows paramagnetically shifted signals in agreement with the presence of a C_{2v} symmetric solution species and indicating the presence of UO_2^+. X-ray quality crystals were obtained from a thf solution of **7**. The X-ray diffraction analysis revealed the presence of the polymeric complex {[UO_2(salophen-^{t}Bu$_2$)(thf)]K(thf)$_2$}$_n$, **8**. An ORTEP view of the [UO_2(salophen-^{t}Bu$_2$)(thf)]K(thf)$_2$ unit is shown in Figure 3 while a view of the coordination polymer **8** is shown in Figure 4. In **8**, the uranium atom is seven coordinated with regular pentagonal bipyramidal coordination geometry. The four donor atoms of the salophen-^{t}Bu$_2^{2-}$ (O_2N_2) and the oxygen of thf form a pentagonal plane (with a mean deviation of 0.0308 Å). The ligand wraps around the uranium adopting a C_s saddle shaped conformation. The axial positions are occupied by two oxo ligands with U═O distances of 1.8534(17) and 1.8491(18) Å, falling in the range of the U═O distances found in **3**, **4** and **6**. The U−$O_{phenolate}$ distances (mean value 2.39(4)Å) are longer and U−N distances (mean 2.59(2) Å) are shorter in comparison with **3**, **4** and **6** complexes. In complex **8**, both oxo groups are involved in a CCI with the K(thf)$_2^+$ ion linking the uranium complexes into a 1D chain with a mean K−O distance of 2.66(4) Å and a U···K···U angle of 139.08(2)°. The K(thf)$_2^+$ ion also coordinates the phenolate oxygen of one [UO_2(Salophen-^{t}Bu$_2$]$^-$ unit (K−O distance of 2.8778(18) Å). The distance between neighboring U ions is 7.63 Å and the U···K···U angle is 139.08°. This results in a smaller separation between U ions than in the polymeric complex {[UO_2py$_5$][KI$_2$py$_2$]}$_n$ (**1**) (9.35 Å) but larger in comparison with [UO_2(salan-^{t}Bu$_2$)(py)K]$_n$ (**3**) (6.63 Å). The presence of a pentavalent uranyl leads to a significant elongation of the mean U−O(salophen-^{t}Bu$_2$) (2.267(7)Å in U(VI) and 2.386(25) Å in U(V)) and mean U−N(salophen-^{t}Bu$_2$) (2.544(5) in U(VI) and 2.598(13) Å in U(V)) distances and of the U═O(oxo) bond lengths (1.782(6) Å in U(VI) and 1.842(7) Å in U(V)) with respect to the previously reported [$U^{VI}O_2$(salophen)(dmf)] complex.[15]

Complex **7** shows full stability in all investigated organic solvents pyridine, dmso, and toluene. These results confirm the important effect of the presence of bulky groups in preventing the disproportionation reaction probably by preventing the formation of the cation−cation intermediate complex. However, a difference in stability was found for the salophen-^{t}Bu$_2^{2-}$ complex as compared to the salan-^{t}Bu$_2^{2-}$ one in some solvents in spite of the similar steric bulk. This suggests that electronic parameters should play an important role in the stability of these complexes. Important differences were also found in the reactivity of these complexes with stoichiometric amounts of water. The reactivity of **3**, **4** and **7** with 1−1000 equiv of water was investigated by NMR spectroscopy. Compound **3** reacts slowly with water in a 1:1 ratio leading to release of the free H_2salan-^{t}Bu$_2$. The reaction proceeds much faster in the presence of 10 equiv of water (few hours) with complete disappearance of the pentavalent species after 24 h. Moreover the reaction of **7** with water shows that no free ligand dissociation or metal oxidation occurs for this complex in the presence of 10 equiv of water up to 30 days and that a very large excess of water is needed before ligand dissociation or metal oxidation occurs. These results suggest that the ligand salophen-^{t}Bu$_2^{2-}$ provides a higher stability of the pentavalent complex with respect to ligand dissociation and metal oxidation as compared to the salan-^{t}Bu$_2^{2-}$. Finally, the addition of 1000 equiv of water to complex **7** leads to oxidation to the hexavalent analogue, but release of free ligand is not observed, suggesting a high stability of this complex with respect to ligand dissociation.

To understand the parameters leading to the stabilization of pentavalent uranyl, we have investigated in detail the spectroscopic and magnetic properties of these complexes and performed a computational study of the electronic structure.

Electronic Structure. The structures of the electronic ground states of the complexes [UO_2py$_5$]$^+$, [UO_2(salan-^{t}Bu$_2$)(py)K], [UO_2(salan-^{t}Bu$_2$)(py)]$^-$, [UO_2(salan)(py)K] and [UO_2(salophen-Me$_2$)(thf)K] were calculated using density functional theory (DFT) approaches. All of the studied structures have been fully optimized in gas phase and in two solvents used in the

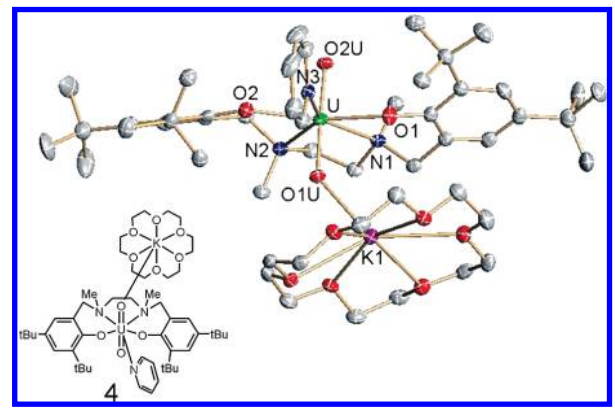

Figure 1. ORTEP view of **4** with thermal ellipsoids at the 30% probability level (hydrogen atoms were omitted for clarity) and schematic representation of the structure.

(34) Mizuoka, K.; Kim, S. Y.; Hasegawa, M.; Hoshi, T.; Uchiyama, G.; Ikeda, Y. *Inorg. Chem.* **2003**, *42*, 1031–1038.

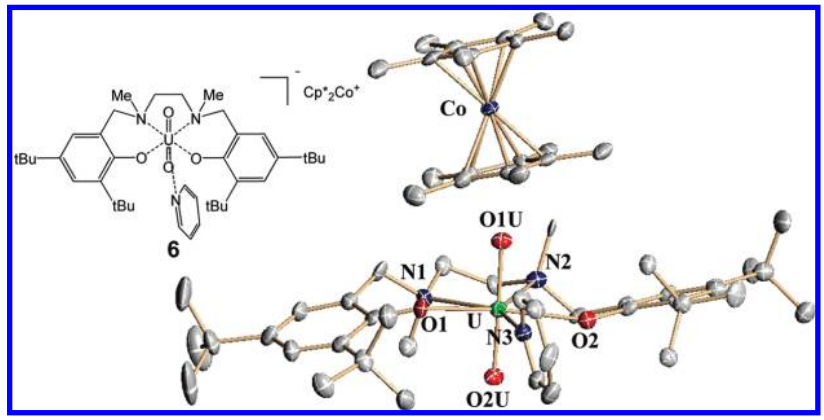

Figure 2. ORTEP view of **6** with thermal ellipsoids at the 30% probability level (hydrogen atoms were omitted for clarity) and schematic representation of the structure.

Table 1. Selected Structural Parameters for **3**, **4**, **6** and **8** (Distances Are Given in Å, Angles in deg.)

structural parameters	$[UO_2(salan\text{-}^tBu_2)(py)K]_n$, **3**	$[UO_2(salan\text{-}^tBu_2)(py)K(18C6)]$, **4**	$[UO_2(salan\text{-}^tBu_2)(py)][Cp^*_2Co]$, **6**	$\{[UO_2(salophen\text{-}\ ^tBu_2)(thf)]K(thf)_2\}_n$, **8**
U−O(1U)	1.819(12)	1.868(2)	1.846(9)	1.8529(18)
U−O(2U)	1.830(12)	1.853(2)	1.866(9)	1.8497(18)
U−O(1)	2.323(11)	2.347(3)	2.388(10)	2.4115(18)
U−O(2)	2.379(11)	2.332(3)	2.371(10)	2.3602(18)
U−N(1)	2.715(16)	2.696(3)	2.773(12)	2.611(2)
U−N(2)	2.690(14)	2.714(3)	2.771(12)	2.586(2)
U−N(3)*	2.618(16)	2.629(3)	2.700(11)	–
U−O(3)*	–	–	–	2.5673(18)
K(1)−O(1U)	2.663(13)	2.651(2)	–	2.6303(19)
O(1)−U−O(2)	178.9(6)	177.38(11)	178.7(4)	177.14(8)

* Coordinated molecule of solvent (pyridine or thf).

Scheme 4

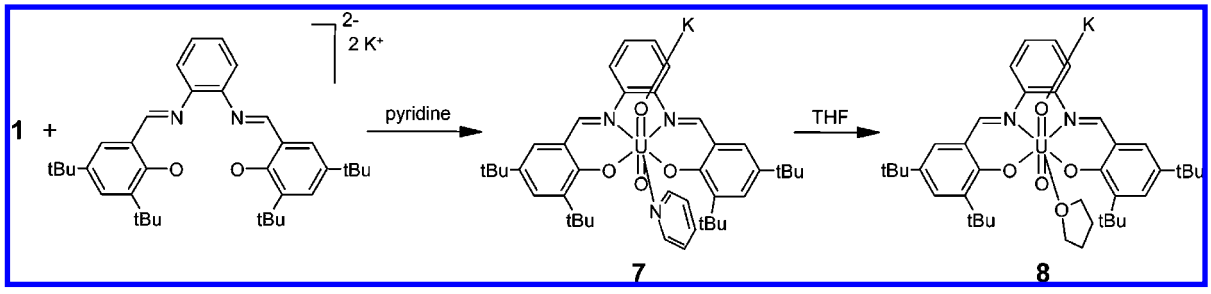

experiments (i.e., pyridine and toluene). In Table 2 we have reported selected computed distances and angles and the corresponding experimental data obtained by X-ray diffraction. Since no significant differences were found between the optimized structural parameters of gas phase and solvated structures, in Table 2 we report only the geometrical parameters obtained in pyridine solvent together with the experimental mean distances (in italics in Table 2), while toluene and gas results are given in the Supporting Information.

It should be underlined that the theoretical structures containing K^+ are somewhat different from the experimental crystallographic structures. For instance, the experimental structures of $[UO_2(salan\text{-}^tBu_2)(py)K]$ and $\{[UO_2(salophen\text{-}^tBu_2)(thf)]K(thf)_2\}$ are polymeric, so that each uranyl oxygen binds one

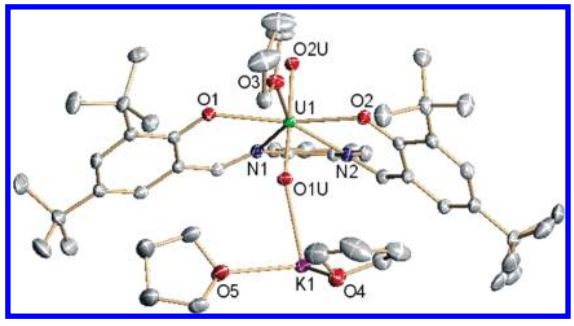

Figure 3. ORTEP view of the coordination environment of the uranyl group in **8** with thermal ellipsoids at the 30% probability level (hydrogen atoms and disorder on thf molecule were omitted for clarity).

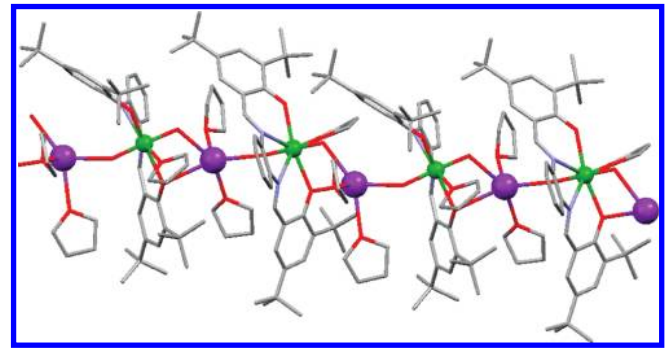

Figure 4. Mercury view of the coordination polymer **8** along the *c* axis.

Table 2. Geometrical Parameters Optimized at the PBE/TZP Level of Theory with Pyridine As Solvent[a]

	U−O_{2u}	U−O_{1u}	O_{2u} −U-O_{1u}	U−O_1	U−O_2	U−N_{1-2}	U-L
UO_2^+	1.80		179.5				
$[UO_2py_5]^+$	1.84 *(1.839)*	1.84 *(1.839)*	179.7				2.61 *(2.614)*
$[UO_2$(salan-^{t}Bu$_2$)(py)$]^-$	1.86 *(1.856)*		178.2 *(178.7)*	2.33 *(2.38)*	2.33 *(2.38)*	2.77 *(2.772)*	2.59 *(2.700)*
$[UO_2$(salan-^{t}Bu$_2$)(py)K]	1.83 *(1.825)*	1.89	178.0 *(178.9)*	2.25 *(2.351)*	2.39 *(2.351)*	2.74 *(2.698)*	2.57 *(2.618)*
$[UO_2$(salan)(py)K]	1.84	1.89	178.3	2.32	2.39	2.80	2.56
$[UO_2$(salophen-Me_2)(thf)K]	1.84*(1.851)*	1.87	178.7	2.30*(2.39)*	2.32	2.58*(2.586)*	2.57*(2.567)*

[a] In italic, experimental mean distances. The numbering of atoms is taken from Figures 1−3. L represents N(pyridine) for the five complexes containing pyridine and O(THF) for the last one.

potassium ion. In our theoretical model, we have used a model structure where just one cation is linked to one of the uranyl oxygens. This leads to a greater dissymmetry in our structures, because the two oxygen atoms in the uranyl unit (U−O) are not equivalent, as for the U−O distances involving the ligand oxygen atoms. As can be seen in Table 2, except for these distances, there is good overall agreement (within 0.01 Å and 1°) between the calculated and experimental structures.

To investigate the nature of the bonding between pentavalent uranyl and the various ligands described in this work and to gain more insight into the origins of the stability of these complexes, we have performed an analysis of the Kohn−Sham molecular orbitals (MO).

The electronic structure of the $[UO_2py_5]^+$ cation arises from an essentially electrostatic interaction between the pyridine ligands acting as σ-donors and the UO_2^+ cation. The MO diagram in pyridine solvent is depicted in Figure 5. The HOMO-1 is a uranyl nonbonding σ MO. Much lower in energy are found the orbitals centered on the ligands. The unpaired alpha electron issuing from the U(V) ($5f^1$) electron doublet configuration is described by an almost degenerate set of two MOs being each occupied by half an electron. They are pure f orbitals, one being of δ-type and the other of ϕ-type, by reference to the labels in uranyl linear symmetry (a representation of the δ, ϕ and π in the uranyl linear symmetry is given in Figure S26, Supporting Information). For the sake of simplicity, this set of two orbitals will be called "degenerate HOMOs" in the following descriptions. The first empty orbital, the LUMO, is a π type f orbital localized on the uranium and is only 0.038 eV higher in energy. Such a picture is consistent with previous multiconfigurational studies.[35,36] For instance, in the case of $[UO_2(CO_3)_3]^{5-}$, the ground state $\sigma^2_u\delta_u$ was found only 403 cm^{-1} (0.049 eV) lower in energy than the first excited state $\sigma^2_u\phi_u$. For the isolated system UO_2^+, the ground state calculated from multiconfigurational CASSCF studies is $88\%\sigma^2_u\phi_u + 12\%\sigma^2_u\delta_u$.[37] In the monodeterminantal DFT scheme, the only way to take into account the almost degenerate nature of the $\sigma^2_u\phi_u$ and $\sigma^2_u\delta_u$ configurations is to allow a fractional occupation of the f(δ) and f(ϕ) orbitals. The energy of these "degenerated HOMOs" obtained from the gas phase calculation and from the calculation in pyridine solvent are respectively −0.5 eV and −5.8 eV. It must be underlined that in both cases the unpaired electron is in a bound state. Nevertheless, the effect of the solvent, here described by a dielectric polarizable medium, on the energy of the MO is very strong for charged species (anions or cations), and all the levels are shifted down to more negative values with respect to the corresponding gas phase MO.

A very different picture is obtained for the salan-^{t}Bu$_2^{2-}$ complexes. As we can see from Figure 5, the MO diagram of the complex $[UO_2$(salan-^{t}Bu$_2$)(py)K] in pyridine solvent exhibits the "degenerate HOMOs" set (−2 eV) higher in energy with respect to the $[UO_2(py)_5]^+$ set (−5.8 eV). The unpaired alpha electron is also in this case located in two "degenerate HOMOs" orbitals each occupied by a half electron. These orbitals result from the combination of one f (δ or π) orbital localized on the metal center with a π* orbital of the pyridine. A significant pyridine π* component (35%−40%) is observed, with a slight variation of this contribution depending on the optimization conditions (gas or solvent). The LUMO orbital is also a δ-type and the first ϕ-type orbital is the LUMO+1, respectively, at 0.18 and 0.24 eV higher with respect to the HOMOs. Moreover, the HOMO-1 orbital is not, as found for the $[UO_2py_5]^+$ system, the nonbonding σ orbital of the UO_2^+ (which is in this case the HOMO-9). The four pairs of unrestricted orbitals located below the HOMO level (identified by a red box on Figure 5) are directly localized on the salan ligand (π-system of the phenolate groups). The presence of a back-donation interaction between the f orbitals of U and the π* orbital of the pyridine, which is not present in the $[UO_2py_5]^+$ species, is consistent with the slight shortening (0.04−0.05 Å) of the bond distance between the uranium and the pyridine ligand in the salan complexes compared to those of the $[UO_2py_5]^+$ complex. Although a comparison of such structurally different compounds is not straightforward, it should be noted that the steric parameters and the charge of the metal ions in the two complexes should lead to shorter U−Npy distances in the cationic $[UO_2py_5]^+$ complex.

The strong π-donor character of the salan-^{t}Bu$_2^{2-}$ ligand (described mainly by a bonding combination of π orbitals of the O atoms with the uranyl MOs), combined with the π-acceptor character of the pyridine ligand thus results in a synergistic effect which stabilizes efficiently the whole edifice. The important effect of this synergistic interaction is supported by the experimental data showing a higher stability of the salan-^{t}Bu$_2^{2-}$ complex in pyridine with respect to other non π-acceptor solvents such as thf.

The participation of 5f orbitals to covalent metal−ligand interactions in U(V) species has been previously reported for organometallic complexes.[38] Notably, DFT studies of uranium(V) imido halide complexes indicated that both U-halide and U═N bonds exhibit covalency with significant participation of the ligand orbitals to the HOMO which contains the f^1 electron.[38]

Another effect of the interaction of the salan-^{t}Bu$_2^{2-}$ ligand with the uranyl group is a slight decrease of the U═O bond strength with respect to the pure UO_2^+ fragment. The computed

(35) Ruiperez, F.; Danilo, C.; Real, F.; Flament, J. P.; Vallet, V.; Wahlgren, U. *J. Phys. Chem. A* **2009**, *113*, 1420–1428.
(36) Gagliardi, L.; Grenthe, I.; Roos, B. O. *Inorg. Chem.* **2001**, *40*, 2976–2978.
(37) Gagliardi, L.; Roos, B. O.; Malmqvist, P. A.; Dyke, J. M. *J. Phys. Chem. A* **2001**, *105*, 10602–10606.
(38) Graves, C. R.; Yang, P.; Kozimor, S. A.; Vaughn, A. E.; Clark, D. L.; Conradson, S. D.; Schelter, E. J.; Scott, B. L.; Thompson, J. D.; Hay, P. J.; Morris, D. E.; Kiplinger, J. L. *J. Am. Chem. Soc.* **2008**, *130*, 5272–5285.

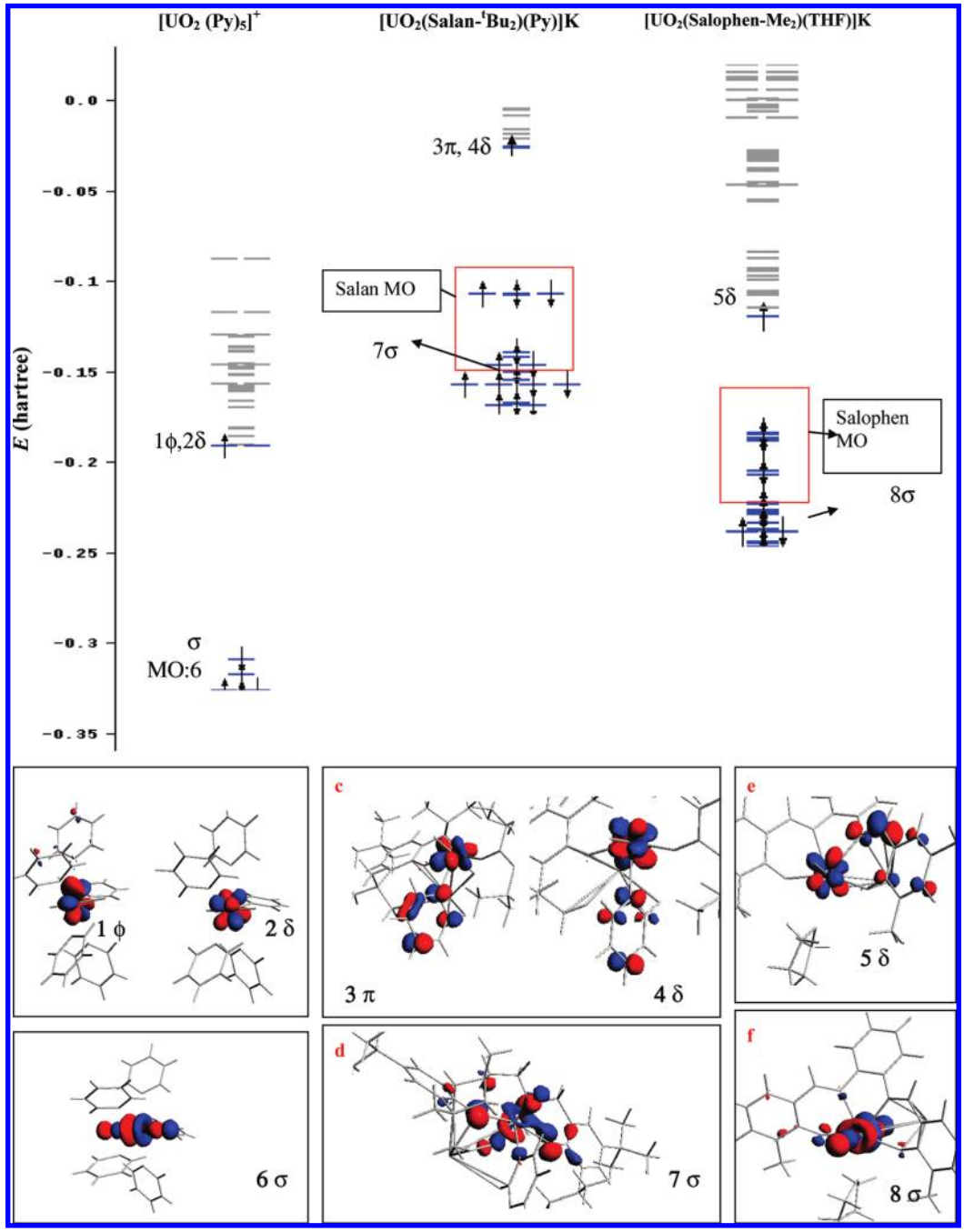

Figure 5. MO diagram of $[UO_2py_5]^+$ $[UO_2(salan\text{-}^tBu_2)(py)K]$ and $[UO_2(salophen\text{-}Me_2)(thf)K]$ complexes. For each complex, the HOMOs (a, c e) and the σ nonbonding uranyl MO are represented (b, d and f). The ϕ, δ, σ and π labels on the graph refer to the symmetry of the f orbitals of the linear uranyl unit.

U−O distances for the isolated uranyl units in the gas phase are 1.77 Å while in the salan-$^tBu_2$ complexes they are between 1.83 and 1.84 Å. Similar distances are found for the $[UO_2py_5]^+$ system. These results are consistent with previous computational studies which have afforded a U−O bond length of 1.742 Å at MRCI level for the isolated UO_2^+ and 1.898 Å (B3LYP-CPCM) for the U−O distance in the $[UO_2(CO_3)_3]^{5-}$ system.[35]

The presence of the potassium ion leads to some variation in the bond lengths with respect to the anionic structure $[UO_2(salan\text{-}^tBu_2)(py)]^-$. Moreover, the potassium ion has an important effect on the energy of the "degenerate HOMOs" set, which we have further investigated. Notably, according to the Koopman's theorem, the energy of the HOMO allows a good estimation of the absolute value of the ionization potential (true in DFT if an exact echange/correlation potential has been used).[39] The optimization of the gas phase anionic structure results in a positive orbital energy of around 1 eV for the degenerate HOMOs. This suggests that the unpaired electron is not bonded to the molecule and that uranyl(V) can easily oxidize to U(VI). In the presence of K^+, all of the levels are shifted down and the "degenerate HOMOs" have energies of around −1.6 eV. When the K^+ ion is placed at the position of the Co ion in the Cp^*_2Co structure (thus with a $K-O_{1u}$ distance of 6.8 Å), the energy of the "degenerate HOMOs" increases (−0.5 eV). In solvent, we observe the same trend (i.e., increase of the HOMO

(39) Koch, W.; Holthausen, M. C. *A Chemist's Guide to Density Functional Theory*; Wiley VCH: Weinheim, 2000.

energy with the increase of the $K-O_{1u}$ distance), but the effect is much weaker. Indeed, as we discussed previously, the dielectric medium stabilizes the charged system, so that the energy of the "degenerate HOMOs" is −1.7 eV for the anionic form and −2 eV with K^+. By varying the position of the K^+ ion to the one corresponding to Co in the Cp^*_2Co compound, we obtained an energy of −1.8 eV.

The cyclic voltammetry (see electrochemistry section and Table 4) of the $[UO_2(salan\text{-}^tBu_2)(py)K]_n$, **3,** $[UO_2(salan\text{-}^tBu_2)(py)K(18C6)]$, **4,** and $[UO_2(salan\text{-}^tBu_2)(py)]$, **5** complexes show that in all cases the same U(VI) species are obtained in the oxidation process. So, in this particular case, we can directly correlate the redox potential of the UO_2^{2+}/UO_2^+ couple in all complexes (from −1.82 to −1.74 V vs Fc^+/Fc) to the computed ionization energy of the unpaired electron in the UO_2^+species. We can observe that when the effect of the cation is reduced by the presence of bound 18C6, the redox potential of the UO_2^{2+}/UO_2^+ couple (−1.81 V vs Fc^+/Fc) is very close to the one found in the absence of potassium (−1.82 V vs Fc^+/Fc for complex **5**). The reduction potential increases to −1.74 V vs Fc^+/Fc when the K^+ is bounded directly to the structure. This is consistent with the increase of the ionization potential in going from structure **5** to **3**. These results clearly point to a significant electronic effect of the potassium counterion in the stabilization of the unpaired electron which leads to an increase of the redox potential of the UO_2^{2+}/UO_2^+ couple.

We have previously reported that the dianionic salan-Me_2^{2-} (salan-Me_2H_2 = *N*,*N*′-bis(2-hydroxybenzyl-3,5-dimethyl)-1,2-dimethylaminomethane) ligand in pyridine leads to the formation of the UO_2^+ complex of salan-Me_2, which rapidly disproportionates to U(IV) and to UO_2^{2+} species.[30] The different reactivity observed in pyridine solution for the pentavalent uranyl complexes of salan-Me_2^{2-} and salan-$^tBu_2^{2-}$ was interpreted in terms of the importance of the steric profile of the *tert*-butyl groups in preventing disproportionation.[30]

To evaluate the effect of the substituents on the phenolate ring on the electronic structure of the resulting pentavalent uranyl complex, we have also studied the structure of $[UO_2(salan\text{-}H_2)(py)K]$. From a geometrical point of view, there are no significant variations in the bond lengths (see Table 2). Moreover, the electronic structure is very similar to the one found for the $[UO_2(salan\text{-}^tBu_2)(py)K]$ complex. As for the ^{t}Bu structure, the "degenerate HOMOs" consists in two orbitals, with eigenvalue of −2 eV, either a f(δ) orbital or f(π), each one combined with a significant pyridine component of π^*. Thus, the ligand substituents, H or ^{t}Bu, have no influence on the electronic structure, suggesting that the higher stability of the $[UO_2(salan\text{-}^tBu_2)(py)K]$ complex in pyridine with respect to the disproportionation reaction is only due to sterical parameters.

Finally, we have analyzed the electronic structure of the Schiff base complex $[UO_2(salophen\text{-}Me_2)(thf)K]$. The main optimized geometrical parameters are collected in Table 2 and the MO diagram is depicted in Figure 5. The HOMO describing the unpaired alpha electron is no longer degenerate. The HOMO is a combination of an f(δ) orbital on U and a π^* orbital (50%) on the N=C Schiff base of the salophen-Me_2 ligand (Figure 5). The empty orbitals show the following ordering: the LUMO is again a f(δ) (0.17 eV higher than the HOMO), the LUMO+1 is the first ϕ-type orbital (+0.32 eV), and the f(π) is the LUMO+2 (+0.36 eV). The energy of the HOMO (−2.7 eV in gas phase, −2.87 eV in toluene and −3.11 eV in pyridine) is lower than the one of the salan-$^tBu_2^{2-}$ ligand (see Figure 5). This is consistent with the higher redox potential measured for the salophen-$^tBu_2^{2-}$ (−1.65 V vs Fc^+/Fc) complex with respect to the salan-$^tBu_2^{2-}$ one (−1.74 V vs Fc^+/Fc). This description is also in agreement with the calculated and experimental bond distances (Table 2), which show a shortening in the $U-N_{ligand}$ bonds (calcd = 2.58 Å, experimental = 2.59 Å) with respect to the salan-$^tBu_2^{2-}$ one (calcd = 2.74 Å, experimental = 2.69 Å). Thus, in this case the two synergistic interactions (π donation from the phenolate oxygen atoms combined with a π-back-bonding interaction with the C=N double bonds) are localized on the salophen-Me_2^{2-} ligand. This is in agreement with the observed stability of the salophen-$^tBu_2$ complex in all solvents and with higher resistance to hydrolysis.

A fragment analysis was performed to compute the energy of the bonding between the uranyl dioxo unit and the ligand (see Figure S13, Supporting Information), which shows that in the gas phase the salophen-Me_2^{2-} is −1.2 eV more strongly bound to the uranyl than the salan-$^tBu_2^{2-}$. In pyridine, the difference is −0.8 eV. This should results in a stronger stability of $[UO_2(salophen\text{-}Me_2)K]$ compared to $[UO_2(salan\text{-}^tBu_2)(py)K]$ with respect to the ligand dissociation reaction.

The qualitative assignment of the magnetic data discussed below is clearly pointing to δ, ϕ as the ground state. It should be noted that in our DFT studies we have used a scalar relativistic approach at 0 K. This approach does not include spin−orbit effects or the probable populations of nearly occupied excited states at higher temperature. Therefore, since the sets of δ, ϕ and π type of f orbitals are close in energy, the description of the exact ordering of these orbitals would need more sophisticated multiconfigurational and spin−orbit approaches. Nevertheless, the latter effects will not change the geometry or the bonding properties of the uranyl complexes that we have obtained by DFT. What should be retained is that the energy of the π orbital in the salophen-$^tBu_2^{2-}$ and the salan-$^tBu_2^{2-}$ complexes is significantly lower than in the $[UO_2py_5]^+$ as a result of the presence of significant back-bonding interaction.

Electronic Spectroscopy. The electronic absorption spectra of the complexes **2**−**7** and **9** have been measured in pyridine solution at room temperature and the data are reported in Table 3. The window of measure was limited to 300−1500 nm because of the pyridine absorption. The assignment of the electronic absorption spectra is not obvious due to the scarcity of experimental and theoretical data in the literature. Spectral studies were reported in dmso for the electrochemically produced mononuclear complexes $[UO_2(salophen)(dmso)]^-$ (with bands at 640, 740, 860, 1470, 1890 nm), $[UO_2(dbm)_2(dmso)]^-$ (with bands at 650, 750, 900, 1400, 1875 nm) and for $[UO_2(CO_3)_2]^{5-}$ (with bands at 760, 990, 1140, 1600, and 1800 nm) in D_2O.[18,34,40] In these compounds the spectral features are very similar to each other in spite of the presence of different ligands coordinated on the equatorial plane and therefore the electronic transitions were assigned to electronic transitions in the UO_2^+ core. The results of theoretical calculations recently performed on these complexes lead the authors to the same conclusion that the observed transitions correspond to transitions in the UO_2^+ core.[35]

The spectra of complexes **5** and **9** are consistent with the presence of a hexavalent uranyl and show characteristic bands that could be assigned to LMCT transition and $\pi \rightarrow \pi^*$ of the ligand. In the pentavalent uranyl complexes, **1**−**4**, **6** and **7**, the bands occurring at wavelengths higher than 500 nm are

(40) Mizuguchi, K.; Park, Y. Y.; Tomiyasu, H.; Ikeda, Y. *J. Nucl. Sci. Technol.* **1993**, *30*, 542–548.

Table 3. UV−Visible, NIR Data for Complexes **2**−**7** and **9** in Pyridine Solution

$U(VI)O_2^{2+}$ complexes			$U(V)O_2^{+}$ complexes		
complex	λ (nm)	ε (cm^{-1} M^{-1})	complex	λ (nm)	ε (cm^{-1} M^{-1})
$[UO_2(salan\text{-}^tBu_2)(py)]$, **5**	390	3800	$\{[UO_2py_5][KI_2py_2]\}_n$, **1**	456	905
	480	3170	$[UO_2py_5]I.py$, **2**	456	1050
$[UO_2(salophen\text{-}^tBu_2)(py)]$, **9**	357	32000		610	110
	432	17400		741	63
			$[UO_2(salan\text{-}^tBu_2)(py)K]_n$, **3**	504	100
				676	25
				850	5
			$[UO_2(salan\text{-}^tBu_2)(py)K(18C6)]$, **4**	513	167
				676	75
			$[UO_2(salan\text{-}^tBu_2)(py)][Cp^*_2Co]$, **6**	505	
			$[UO_2(salophen\text{-}^tBu_2)(py)K]$, **7**	423	20000
				632	200
				726	314
				853	363
				1431	170

consistent with f−f transitions and with the presence of a $5f^1$ configuration while the bands below 500 nm can be assigned to LMCT transition or to $\pi \rightarrow \pi^*$ of the ligand. The $\pi \rightarrow \pi^*$ transition of the salophen-$^tBu_2^{2-}$ ligand in equatorial position is located for **7** and **9** in the range 423−432 nm. The absorption spectrum of the complex **7** shows the expected bands assigned to f−f transitions and the observed ε values and peak position are comparable to those previously describes by Ikeda for the $[UO_2(salophen)(dmso)]^-$ complex in dmso solution.[18] The absorption spectra of the complexes **3** and **4** are very similar with close peak positions (∼505 nm, ∼675 nm) and very similar ε values in agreement with the expected presence of analogous structures in solution. The band at ∼850 nm could not be observed for **4** because of the very small ε. These bands were assigned to Laporte forbidden f−f transitions. The spectrum of **6** presents an additional band at ∼505 nm but the ε value was difficult to determinate because of the presence of several species in solution which contribute to the global absorbance. However, the shape of the spectrum confirms the presence of UO_2^+ complex as the major product in pyridine solution. Interestingly, the ε values for the complexes **3** and **4** are smaller than those of **7** in spite of the similar symmetry of the coordination geometry of the solution species (pentagonal bipyramid). This could be explained by a strong overlap of the metal and the ligand orbitals in the case of **7** which partially allows the transition. This is in agreement with the computed electronic structure of **7**. The spectra of **1** and **2** show a band at 456 nm which is difficult to assign because the ε value is higher than those interpreted as Laporte forbidden f−f transitions but could be interpreted as a charge-transfer band. The two other bands observed in the case of **2** (610 and 741 nm) can be assigned as f−f transitions. Theoretical computation will be needed to confirm this assignment.

Electrochemistry. The values of the redox potentials UO_2^{2+}/UO_2^+ couple provide a direct measure of the stability of the isolated pentavalent complexes with respect to the oxidation reaction to the hexavalent analogue. Therefore the influence of different parameters as the structure of the supporting ligand or the presence of coordinating cations on the stability of the UO_2^+ species can be directly probed by cyclic voltammetry experiments. The solution redox properties of the complexes **2**−**5**, **7** and **9** have been studied by cyclic voltammetry in pyridine solution and the respective values of the $E_{1/2}$ (V) of the couple vs the couple Fc^+/Fc are listed in Table 4.

The cyclic voltammogram of the complex **3** reveals a nearly reversible redox feature at $E_{1/2} = -1.74$ V vs Fc^+/Fc. This is

Table 4. Summary of Redox Potential Data for Complexes **2**−**5**, **7** and **9** in ∼0.1 M $[NBu_4][PF_6]$/Pyridine Solution at Room Temperature[a]

complex	$E_{1/2}$ (U^{VI}/U^V) V)	$\Delta E_{p,100mV/s}$ (V)
$[UO_2py_5]I.py$, **2**	−0.91, −0.46	
$[UO_2(salan\text{-}^tBu_2)(py)K]_n$, **3**	−1.74	0.13
$[UO_2(salan\text{-}^tBu_2)(py)K(18C6)]$, **4**	−1.81	0.14
$[UO_2(salan\text{-}^tBu_2)(py)]$, **5**	−1.82	0.18
$[UO_2(salophen\text{-}^tBu_2)(py)K]$, **7**	−1.65	0.13
$[UO_2(salophen\text{-}^tBu_2)(py)]$, **9**	−1.67	0.09

[a] Potential values are given vs the Fc^+/Fc couple.

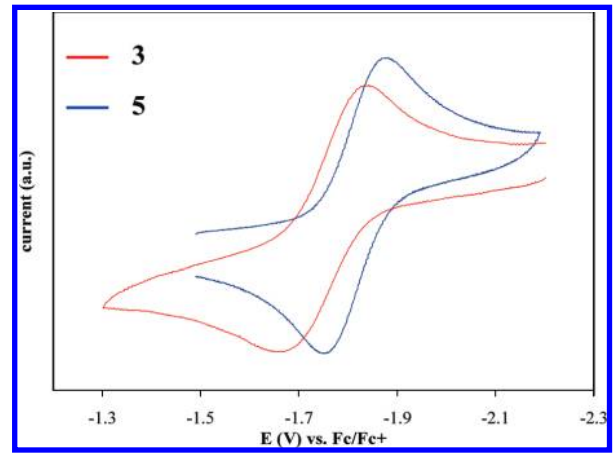

Figure 6. Room temperature cyclic voltamogramm for **3** and **5** in pyridine at 100 mV/s (0.1 M $[NBu_4][PF_6]$ as supporting electrolyte).

in the range of the UO_2^{2+}/UO_2^+ potential measured in anhydrous solutions (−1.3 V/−1.82 V, vs Fc^+/Fc).[20,41] To evaluate the influence of a coordinated countercation, in this case the potassium ion, the redox properties of **5** ($E_{1/2} = -1.82$ V vs Fc^+/Fc) were also studied in the same conditions. The small but significant differences in term of potential (Figure 6) between the two complexes indicates that the potassium does have an influence even in the presence of a large excess of the $[NBu_4]^+$ cation. These results indicate that the coordination of the potassium in pyridine solution results in the stabilization of the uranyl(V) complex with respect to the oxidation reaction. This compares well with the NMR experiments and DFT calculations. No significant stabilizing effect was found in the presence of the less coordinating cation $(K18C6)^+$.

(41) Hayton, T. W.; Boncella, J. M.; Scott, B. L.; Batista, E. R.; Hay, P. J. *J. Am. Chem. Soc.* **2006**, *128*, 10549–10559.

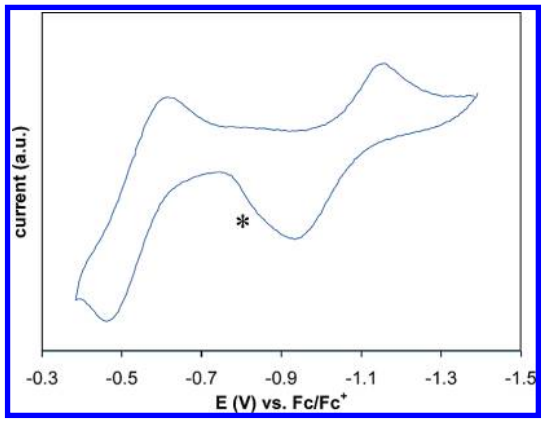

Figure 7. Room temperature cyclic voltammogram for **2** in pyridine at 10 mV/s (0.1 M $[NBu_4][PF_6]$ as supporting electrolyte, * impurity).

The cyclic voltammograms of the salophen-^{t}Bu$_2^{2-}$ complexes **7** and **9** reveal reversible redox features at similar $E_{1/2}$ values (−1.65 and −1.67 V vs Fc^+/Fc respectively) without significant effect of the potassium coordination being observed for this system. These values are lower than those measured for the complex $[UO_2$(salophen)(dmso)] (−1.55 V vs Fc^+/Fc) in dmso.[34] The difference can be attributed to the difference in the coordinated solvent (pyridine or dmso) or/and to the presence of *tert*-butyl groups. The $\Delta E_{1/2}$ difference between the salophen-^{t}Bu$_2^{2-}$ and the salan-^{t}Bu$_2^{2-}$ complexes (0.15 V) unambiguously indicates a higher stability of the UO_2^+ complex of salophen-^{t}Bu$_2^{2-}$ with respect to the oxidation reaction.

The cyclic voltammogram of the complex **2** (Figure 7) is more complicated and reveals two redox features at $E_{p,a} = -0.93$ V vs Fc^+/Fc and $E_{p,a} = -0.46$ V vs Fc^+/Fc. The presence of two features suggests the presence of two UO_2^+ species in the pyridine solution. The ΔE_p are respectively 0.16 and 0.23 V at 10 mV/s and increase rapidly with increasing the scan speed suggesting a slow kinetics of the electron transfer which are usually associated with structural rearrangements.[11] In this case, the presence of an exchange in pyridine solution between species with or without coordinated iodide could be responsible for the observed behavior. The values of the UO_2^{2+}/UO_2^+ potential were found to be much higher than those measured for the complexes **3**, **4** and **7** in agreement with the DFT calculation. This difference in redox potential is likely to play a role in the observed stability in pyridine solution of **1** and **2**, which do not present bulky groups preventing the disproportionation through a cation−cation complex formation.

Magnetic Properties. The fundamental understanding of the molecular parameters governing magnetic exchange interactions and electron delocalization in molecular compounds of actinides remain very limited.[42−44] The $5f^1$ ions are particularly useful for the interpretation of magnetic data because electron repulsion is absent. However the scarcity of reported U(V) complexes has limited the number of magnetic studies on this oxidation state to simple salts and few organometallic complexes.[38,42,45−49] The magnetic data for UO_2^+ complexes are limited to three examples[27,28] which include our report of complexes presenting an unambiguous $UO_2^+\cdots UO_2^+$ interaction. The solid state temperature-dependent magnetic susceptibility of complex **1** had been also described[28] (see Figure S22, Supporting Information) and was found to be very similar to that of the dinuclear macrocyclic complex presenting a $UO_2^+\cdots$Zn interaction reported by P. Arnold et al.[27] Temperature-dependent magnetic susceptibility data were collected for the isolated complexes **4** and **7** from 5 to 300K and are given in Figure S22, Supporting Information. Samples of **4** and **7** display effective magnetic moments that vary with temperature reaching an effective magnetic moment of respectively 2.20 μ_B and 2.23 μ_B at 300 K. The effective moments in pyridine solution (at 300K) were also measured for **4** and **7** by the Evans method[50] and were found to be in agreement with those measured in the solid state (i.e., respectively $\mu_{eff} = 2.25(10)\ \mu_B$ and $\mu_{eff} = 2.14(10)\ \mu_B$). The very low solubility of **1** in pyridine renders it impossible to measure the effective moment by the same method. However, the effective moment in solution was measured for the soluble complex **2** and was found to be $\mu_{eff} = 2.6(1)\ \mu_B$. This is in agreement with the value measured for **1** in the solid state ($\mu_{eff} = 2.57\ \mu_B$).[33] While the theoretical effective magnetic moment calculated for a free $5f^1$ ion in the L−S coupling scheme is $\mu_{eff} = 2.54\ \mu_B$[51] the range of the effective magnetic moment values reported for U(V) complexes is large (1.42−2.57 μ_B)[27,38,45−47,49,52−55] indicating that the coordination sphere has an important influence on the magnetic moment. Important differences are observed between the magnetic data of complexes **4** and **7** and those of complex **1** and **2**. Notably complex **1** in the solid state and complex **2** in solution show higher values of the effective magnetic moment at room temperature ($\mu_{eff} = 2.57\ \mu_B$ and $\mu_{eff} = 2.6(1)\ \mu_B$, respectively) which are very close to the theoretical value for an isolated $J = 5/2$ multiplet.

Plots of the magnetic μ_{eff} data vs T (Figure S22, Supporting Information) decreases for complexes **4** and **7** with decreasing temperature as it was observed for **1.**[28] However, a significant difference is observed in the low-temperature susceptibilities (<50 K). The results of the DFT calculation indicate that for both complexes **4** and **7**, the HOMO (SOMO) is an f−π* admixture whereas for **1** the SOMO is a pure f orbital. This might indicate that the value of the effective moment is influenced by the nature of the SOMO.

EPR measurements can provide important information on the nature of metal−ligand bonding but only a very limited number of EPR data have been reported for U(V) compounds.[48,49,54,55,56] In addition, several uranium(V)imido complexes have been reported to be EPR silent due to their $\mu = \pm 3/2$ crystal-field ground state.[45,47,52,54] Gourier and co-workers[48] concluded from a detailed comparative EPR study of the electronic structure of

(42) Edelstein, N. M.; Lander, G. H. *Magnetic properties*; Springer: Dordrecht, 2006.
(43) Clark, D. L.; Hecker, S. S.; Jarvinen, G. D.; Neu, M. P. *The Chemistry of the Actinide and Transactinide Elements*; Springer: Dordrecht, 2006.
(44) Schelter, E. J.; Morris, D. E.; Scott, B. L.; Thompson, J. D.; Kiplinger, J. L. *Inorg. Chem.* **2007**, *46*, 5528–5536.
(45) Rosen, R. K.; Andersen, R. A.; Edelstein, N. M. *J. Am. Chem. Soc.* **1990**, *112*, 4588–4590.
(46) Selbin, J.; Ortego, J. D. *Chem. Rev.* **1969**, *69*, 657–671.
(47) Castro-Rodriguez, I.; Olsen, K.; Gantzel, P.; Meyer, K. *J. Am. Chem. Soc.* **2003**, *125*, 4565–4571.
(48) Gourier, D.; Caurant, D.; Berthet, J. C.; Boisson, C.; Ephritikhine, M. *Inorg. Chem.* **1997**, *36*, 5931–5936.
(49) Bart, S. C.; Anthon, C.; Heinemann, F. W.; Bill, E.; Edelstein, N. M.; Meyer, K. *J. Am. Chem. Soc.* **2008**, *130*, 12536–12546.
(50) Evans, D. F. *J. Am. Chem. Soc.* **1959**, 2003–2005.
(51) Boudreaux, E. A.; Mulay, L. N. *Theory and Applications of Molecular Paramagnetism*; Wiley: New York, 1976.
(52) Brennan, J. G.; Andersen, R. A. *J. Am. Chem. Soc.* **1985**, *107*, 514–516.
(53) Castro-Rodriguez, I.; Nakai, H.; Meyer, K. *Angew. Chem., Int. Ed.* **2006**, *45*, 2389–2392.
(54) Meyer, K.; Mindiola, D. J.; Baker, T. A.; Davis, W. M.; Cummins, C. C. *Angew. Chem., Int. Ed.* **2000**, *39*, 3063–3066.
(55) Gourier, D.; Caurant, D.; Arliguie, T.; Ephritikhine, M. *J. Am. Chem. Soc.* **1998**, *120*, 6084–6092.

Table 5. Summary of Magnetic Data

complex	μ_{eff} (300K)	μ_{eff} (6K)	EPR data (4K)
$\{[UO_2py_5][KI_2py_2]\}_n$, **1**	2.57	0.80	No signal in the solid state No signal in dilute solution (5×10^{-4}M)
$[UO_2py_5]I.py$, **2**	2.6(1)[b]	–	No signal
$[UO_2(salan\text{-}^tBu_2)(py)K]_n$, **3**	2.35[b]	–	$g_x = 1.94$; $g_y = 0.98$; $g_z = 0.75$
$[UO_2(salan\text{-}^tBu_2)(py)K(18C6)]$, **4**	2.20[a] 2.25(10)[b]	1.05	$g_x = 1.98$; $g_y = 1.25$; $g_z = 0.74$
$[UO_2(salophen\text{-}^tBu_2)(py)K]$, **7**	2.23[a] 2.14(10)[b]	0.72	Very broad signal (no fit possible)
$[UO(OSiMe_3)(thf)Zn_2I_2(L)]$ (ref.[27])	2.38[a]		$g = 2.2$ (5K in frozen methyl THF sol.)

[a] Solid state. [b] Solution.

organouranium(V) amide and alkoxide compounds that in amide complexes the 5f orbital is essentially non bonding but a covalent character appears for the interaction of 5f orbitals with oxygen ligands. To obtain more details of the electronic structure of the complexes **1**, **3**, **4** and **7**, X-band EPR spectroscopy was performed at low temperature. The results of EPR measurements are summarized in Table 5 and spectra are shown in the Supporting Information.

Recent theoretical calculations for the gas phase UO_2^+ ion including spin−orbit coupling show that the six lowest energy states are derived from the 5fδ_u, 5fϕ_u, and 5fπ_u orbitals, well-separated from the next higher lying state corresponding to the first oxygen to uranium charge transfer state.[31] Further calculations (including spin−orbit coupling) for the $[UO_2(CO_3)_3]^{5-}$ complex indicate that the first four states in the complex also correspond to states that come from the nonbonding 5fδ and 5fϕ orbitals in the UO_2^+ free ion. Interestingly, these calculations show a significant decrease in the energy of the π_u* orbital in the complex compared to the free gas phase UO_2^+ ion, (19049 cm^{-1}) to 7467 cm^{-1} (complex, gas phase) or 7444 cm^{-1} (complex, solution), attributed in this paper to much lower oxygen 2p character from the yl-oxygen resulting in a less antibonding π* orbital. Our calculations discussed earlier suggest extensive π bonding between the pyridine molecule and uranyl(V) orbitals in the salan-$^tBu_2^{2-}$ complex.

As discussed above, the four lowest states are derived from the nonbonding 5f ϕ and δ orbitals and it is these states which determine the measured magnetic properties of the uranyl(V) complexes. Inclusion of the π* orbital within a few hundred cm^{-1} of the ground state would not markedly affect the model calculation that follows. Thus crystal field theory can be utilized to calculate, at least qualitatively, the magnetic properties of uranyl(V) complexes for the temperature range from 0 to 300 K, corresponding to an energy range of 0 to ~200 cm^{-1}.

Equatorial coordination of the uranyl(V) ion introduces an equatorial crystal field which could mix the $J_z = \pm 5/2$ and $J_z = \pm 3/2$ states (see Figure 8). The UO_2^+ ion in **1** and **2** has five pyridine molecules surrounding the U ion in the equatorial plane and the five nearest neighbor nitrogen atoms are in the equatorial plane. Assuming that these nearest neighbor nitrogen atoms are the major contribution to the equatorial crystal field potential the symmetry of this potential is D_{5h}. When spin−orbit coupling is included the low-lying free ion δ and ϕ states are mixed and the "good" quantum number in the SLJJz representation is $\pm J_z$. This is shown schematically in Figure 8. For $|g_\perp| > 0$, the doubly degenerate ground state wave function must contain a mixture of J_z values that differ by ± 1. In an equatorial field of D_{5h} symmetry this mixture of J_z states is not possible so $g_\perp = 0$. Since the intensity of the EPR signal is proportional to $g_\perp^2$, there should be no signal observed for **1** and **2**.

For compounds **3**, **4**, and **7** listed in Table 5, again considering only the nearest neighbors, the site symmetry at the uranium ion in the equatorial plane is at least C_2, which means that there are B_2^2,B_2^4,B_4^4,B_2^6,B_4^6,B_6^6 terms in the crystal field potential. Assuming the δ and ϕ states are relatively close, then only the fourth order terms, B_4^4 and B_4^6, could mix the J_z states shown in column B in Figure 8, to lead to a nonzero value for $g_\perp$. In the, Supporting Information we present a qualitative calculation for the g values vs the relative energies of the δ and ϕ states.

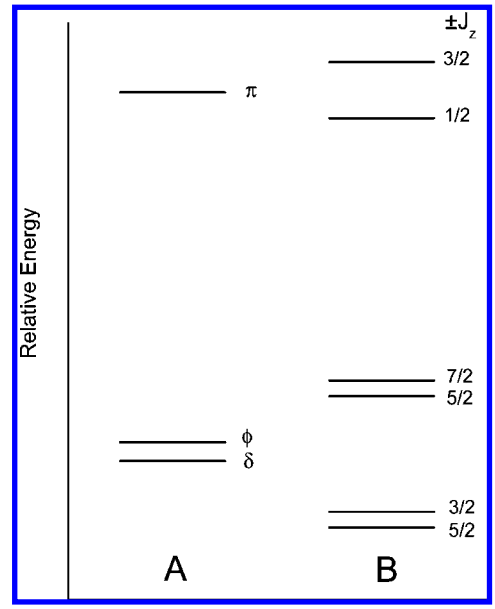

Figure 8. Schematic energy level diagram of the 5f orbitals for the uranyl(V) free ion. It is assumed the axial crystal field is the strongest interaction. Column A shows the relative energies of 5f orbitals. The 5fσ antibonding orbital is not shown as it is shifted to much higher energy. Column B gives the relative energies when spin−orbit coupling is included. The levels in B are each doubly degenerate, a linear combination of $^2F_{5/2}$ and $^2F_{7/2}$ basis states, and labeled by the J_z quantum number.

Qualitatively, the EPR data for **3**, **4**, and **7** can be approximately fit with this simple model when $g_{||} \approx 2$, $g_\perp \approx 1.3$ (assuming $g_{||} = |g_1|$, and $g_\perp \approx (|g_2 + g_3|)/2$) and $(\epsilon_\delta - \epsilon_\phi) = -1435$ cm^{-1}, see, Supporting Information). It is interesting to note that the EPR data for $[UO(OSiMe_3)(thf)Zn_2I_2(L)]$[27] can also be qualitatively fit with this model if we assume their measured g value of 2.20 is g_1 (or $g_{||}$), and that g_2 and g_3 are too broad to be determined. The temperature dependence of the magnetic susceptibility data also suggest that one or more excited states are relatively low-lying, that is within a few hundred cm^{-1}.

Conclusions

In this work, we have presented the synthesis, magnetic and redox properties, reactivity and the DFT analysis of the electronic structure and bonding for a series of stable complexes of pentavalent uranyl containing ligands with very different steric and electronic properties. The cationic complex $[UO_2py_5]^+$

(56) Edelstein, N.; Brown, D.; Whittaker, B. *Inorg. Chem.* **1974**, *13*, 563.

has in the equatorial plane five weakly bound pyridine ligands acting as σ-donors only, with the f unpaired electron localized in a isolated metal orbital. The high stability of this complex is probably the result of the high redox potential that makes the oxidation of this species to the hexavalent analogue in pyridine solution difficult. The high stability of this species in pyridine disfavors the disproportionation reaction even in the absence of bulky ligands. The weakly associated pyridine ligands can be easily replaced by π-donor ligands such as the aminophenolate salan ligands and the Schiff-base salophen ligands. However, these ligands are not able to stabilize pentavalent uranyl with respect to the disproportionation reaction in the absence of bulky substituents which can disfavor the formation of dimeric intermediates. As a result, the reaction of $\{[UO_2py_5][KI_2py_2]\}_n$ with salophen^{2-} or with salan-Me$_2^{2-}$ leads to unstable species which rapidly disproportionate to form U(IV) and UO_2^{2+} species. Conversely the highly stable complexes [UO_2(salan-^{t}Bu$_2$)(py)K] and [UO_2(salophen-^{t}Bu$_2$)(py)K] can be prepared in pyridine solution. The magnetic and the EPR data can be qualitatively analyzed with a simple crystal field model where the f electron has a nonbonding character. However, the DFT studies show unambiguously the presence of a significant covalent contribution to the metal−ligand interaction in these complexes leading to a significant lowering of the π_u*. These two results are not contradictory because the presence of π* orbital within a few hundred cm^{-1} of the ground state would not markedly affect the model calculation used to analyze the magnetic data. Moreover, the temperature dependence of the magnetic susceptibility data also suggests that one or more excited states are relatively low-lying, that is within a few hundred cm^{-1}. The presence of the back-bonding interaction is likely to play a role in the stabilization of pentavalent uranyl both with respect to the disproportionation reaction and to the hydrolysis reaction. Notably, in spite of the presence of ligands with similar steric hindrance, the stability of the salan-^{t}Bu$_2$ complex with respect to the disproportionation is reduced in solvents other than pyridine, but the salophen-^{t}Bu$_2$ complex is fully stable in all organic solvents. Moreover, the [UO_2(salophen-^{t}Bu$_2$)(py)K] complex shows a higher stability than [UO_2(salan-^{t}Bu$_2$)(py)K] with respect to the oxidation reaction as evidenced by its higher redox potential and a much higher stability with respect to the reaction of ligand dissociation promoted by stoichiometric amounts of water. Finally, cations which can coordinate the yl-oxygens of the pentavalent uranyl moiety play also an important role on the overall electronic structure and stability of the complex. This is clearly shown by the DFT studies and by the measured redox potential which is significantly decreased for the salan-^{t}Bu$_2$ complexes in the absence of the coordinating potassium cation. These results provide an unprecedented complete description of the structure and bonding in stable pentavalent uranyl complexes. The overall picture indicates that complexes of pentavalent uranyl fully stable in organic solution and resistant to hydrolysis can be prepared by a careful tuning of both steric and electronic properties of the supporting ligand coupled to an appropriate choice of counterions. These results should promote the expansion of the coordination chemistry of pentavalent uranyl and suggest that a careful ligand design might also lead to higher stability with respect to hydrolysis.

Experimental Section

General Procedures. All manipulations were carried out under an inert argon atmosphere using Schlenk techniques and an MBraun glovebox equipped with a purifier unit. The water and oxygen levels were always kept at less than 1 ppm. The solvents were purchased from Aldrich in their anhydrous form, conditioned under argon and vacuum distilled from K/benzophenone (pyridine, thf, hexane and diisopropylether) or CaH_2 (acetonitrile). Commercial anhydrous dmso-d_6 was further dried over molecular sieves preliminary heated at 200 °C. Depleted uranium turnings were purchased from the "Société Industrielle du Combustible Nucléaire" of Annecy (France). Pyridine N-oxide and 18-crown-6 (18C6) were purchased from Aldrich and dried under vacuum at 50 °C for 7 days. Elemental analyses were performed under argon by Analytische Laboratorien GMBH at Lindlar, Germany. FTIR spectra were recorded with a Perkin-Elmer 1600 Series FTIR spectrophotometer. UV−visible measurements were carried out with a Varian Cary 50 Probe spectrophotometer and a Lambda 9 Perkin Elemer spectrophotometer in quartz cells (optical path lengths: 1 mm and 1 cm) adapted with J. Young valves.^{1}H NMR spectra were recorded on Varian UNITY and MERCURY 400 MHz and Bruker 200 MHz spectrometers. NMR chemical shifts are reported in ppm with solvent as internal reference.

Methods. Static magnetic properties were measured using a Quantum Design SQUID MPMS-XL 5.0 susceptometer. Ultra-Low Field Capability ± 0.05 G for the 5 T magnets. Continuous Low Temperature Control/Temperature Sweep Mode (CLTC) - Sweep rate: 0.001 - 10 K/min. The samples were pressed under argon into a Kel-F or an aluminum container which was then sealed under vacuum in a 5 mm Suprasil-Quartz tube. Contribution to the magnetization from the Kel-F or the aluminum container and tube were measured independently and subtracted from the total measured signal. Diamagnetic corrections were made using Pascal's constants. At 300 K, we calculated a μ_{eff} of 2.20 μ_B for **4** ($\chi_{dia} = -7.68 \times 10^{-4}$ emu/mol, $m = 25.81$ mg, $M = 2037.08$ g/mol). At 300 K, we calculated a μ_{eff} of 2.23 μ_B for **7** ($\chi_{dia} = -5.46 \times 10^{-4}$ emu/mol, $m = 15.60$ mg, $M = 1147.78$ g/mol).

Cyclic voltammetry experiments were performed using a PAR 273 potentiostat. All experiments were performed in a glovebox. The working electrode consisted of a platinum disk embedded in PTFE (1 mm diameter or 2.5 mm diameter), a Pt counterelectrode, and an Ag/AgCl reference electrode. Solutions employed during cyclic voltammetry studies were typically 2.5 mM in the uranium complex and 0.1 M in [Bu_4N][PF_6]. All potentials are reported versus the [Cp_2Fe]$^{0/+}$ couple.

The EPR measurements were performed in quartz tubes with J.Young valves. EPR spectra at X-band were recorded with an EMX Bruker spectrometer fitted with an OXFORD Instrument ESR900 cryostat. All spectra were recorded under unsaturated conditions with the following set of parameters: $T = 4$K, $P = 3.17$ μW, amplitude modulation 9G, frequency modulation 100 kHz.

Computational Methods. The theoretical study of uranium complexes has been performed with the ADF2007 DFT code.[57−59] A GGA functional (namely PBE) has been chosen combined with Triple-ζ Slater type orbital (STO) valence basis sets. The core density was generated for all atoms from four-components Dirac−Slater calculations and then kept frozen in molecular computations. The valence space includes the 6s, 6p, 6d, 5f, 7s orbitals plus one 7p polarization function for U and 2s, 2p orbitals plus 3d polarization function for K, N, C and O. The corresponding auxiliary sets of STO functions were used for all the atoms to fit the molecular density and to generate the Coulomb and exchange potentials. The scalar relativistic corrections were included in the valence space via the ZORA formalism. All calculations have been performed in an unrestricted formalism for the ground doublet state of U(V). Solvent effects have been computed with a Polarizable

(57) Velde, G. T.; Bickelhaupt, F. M.; Baerends, E. J.; Guerra, C. F.; Van Gisbergen, S. J. A.; Snijders, J. G.; Ziegler, T. *J. Comput. Chem.* **2001**, *22*, 931–967.
(58) Boerrigter, P. M.; Velde, G. T.; Baerends, E. J. *Int. J. Quantum Chem.* **1988**, *33*, 87–113.
(59) Baerends, E. J.; Ellis, D. E.; Ros, P. *Chem. Phys.* **1973**, *2*, 41–51.

Continuum Model using the COSMO routine in ADF and molecular orbital pictures obtained by the ADF graphical user interface. The description of the M-ligand bonding was achieved by the symmetry fragment-based construction of KS molecular orbitals (MO) in ADF: the final MO's are built as linear combinations of symmetrized-fragment orbitals (SFOs) in the molecular symmetry.

Syntheses. $[UI_3(thf)_4]$[60] and $[UI_4(PhCN)_4]$[61] were synthesized as previously described. The synthesis of the pentavalent uranyl complexes $\{[UO_2py_5][KI_2py_2]\}_n$, (**1**) and of $[UO_2(salan\text{-}^tBu_2)(py)(K)]_n\cdot 2KI$ (**3**)[22,33] and of the hexavalent uranyl complexes $[UO_2(salan\text{-}^tBu_2)(py)]$ (**5**), $[UO_2(salophen)(py)]$ (**10**) were performed according to the previously described procedure.[22,33]

Isolation of $[UO_2py_5]$I.Py (2). $\{[UO_2py_5][KI_2py_2]\}_n$ (30.0 mg, 0.027 mmol, 1 equiv) was added to a stirred solution of 18-crown-6 (18C6) (7.8 mg, 0.030 mmol, 1.1 equiv) in pyridine (0.6 mL). The resulting red solution was filtered. Then, $^iPr_2O$ (8 mL) was slowly added, resulting in the immediate formation of a rust colored solid. The solid was subsequently washed 3 times with 3 mL of $^iPr_2O$ and dried under vacuum (20 mg). Anal. calcd for $[UO_2py_3]$-I.K(18C6)I, $C_{27}H_{39}N_3O_8I_2KU$: C, 30.46; H, 3.69; N, 3.95. Found: C, 29.11; H, 3.75; N, 3.80.

The presence of KI(18C6) salts, which are very difficult to separate, does not allow to rule out the presence of traces of polymeric complex in the bulk compound, but the absence of starting polymer was confirmed by a comparison of the IR spectra.

Red crystal (blocks) of **2** suitable for X-ray diffraction studies were obtained by slow diffusion over a 3 weeks period of hexane into a 2×10^{-2} M pyridine solution of $\{[UO_2py_5][KI_2py_2]\}_n$.

Synthesis of $[UO_2(salan\text{-}^tBu_2)(py)(K18C6)]$ (4). A solution of 18-crown-6 (18C6) (105 mg, 0.400 mmol, 3.3 equiv) in toluene (4 mL) 104.0 mg (0.120 mmol, 1 equiv) was rapidly added to a freshly prepared (to avoid decomposition) pink suspension of $[UO_2(salan\text{-}^tBu_2)(py)K]_n\cdot 2KI$ in toluene (2 mL), resulting in a violet solution. After 5 min of stirring, a violet solid formed, which was filtered, washed 3 times with 3 mL of toluene and dried under vacuum (104 mg, 55% yield) Anal. calcd for $[UO_2(salan\text{-}^tBu_2)(py)(K18C6)]$. 2K(18C6)I, $C_{75}H_{131}UN_3O_{22}K_3I_2$: C, 44.24; H, 6.49; N, 2.06. Found: C, 44.24; H, 6.45; N, 2.05.

The amount of cocrystallized K(18C6)I can be reduced if the reaction of $[UO_2(salan\text{-}^tBu_2)(py)K]_n\cdot 2KI$ with excess crown ether is carried out in pyridine. The complex $[UO_2(salan\text{-}^tBu_2)(py)$-(K18C6)].K(18C6)I can be isolated by addition of n.hexane to pyridine followed by recrystallization in toluene.

^{1}H NMR (Pyridine-d_5; 298 K; 400 MHz): Two sets of signals corresponding to isomers C_2 and C_s in the ratio 100:9 were found. First set (**I**): −12.62 (br, 2H, $-NCH_2-$); −10.09 (br, 2H, $-NCH_2-$); −8.35 (s, 3H, $-N(CH_3)-$); −6.39 (br, 2H, -NCH_2-Ph); −4.74 (s, 18H, −*t*Bu); 0.18 (s, 18H, -*t*Bu); 3.06 (s, 2H, $-CH-_{aromatic}$); 4.62 (s, 2H, $-CH\text{-}_{aromatic}$); 5.70 (s, 2H, $-CH_2O-$) 11.49 (br, 2H, $-NCH_2-$Ph). Second set (**II**): −12.89 (br, 2H, $-NCH_2-$); −8.46 (br, 2H, -NCH_2-Ph) −6.52 (s, 3H, $-N(CH_3)-$); −5.57 (br, 2H, $-NCH_2-$); −3.42 (s, 18H, $-^tBu$); 0.24 (s, 18H, $-^tBu$); 2.82 (s, 2H, $-CH-_{aromatic}$); 4.91 (s, 2H, $-CH-_{aromatic}$); 6.00 (br, 2H, $-NCH_2-$Ph).

Violet crystals suitable for X-ray diffraction were obtained by letting stand at room temperature a solution of **3** reacted with 18C6 (3.2 mg, 1.1 equiv per K^+) in 0.7 toluene-d_8.

Isolation of $[UO_2(salan\text{-}^tBu_2)(py)][Cp^*_2Co]$ (6). Cp^*_2Co (24.8 mg, 1.5 equiv) was added to a red pyridine solution (2 mL) of $[UO_2(salan\text{-}^tBu_2)(py)]$ (43.8 mg, 1 equiv). The resulting red suspension was stirred for 16 h at room temperature. The resulting clear orange solution was filtrated and the solvent was evaporated to 0.5 mL. Then, the solution was let standing for 16 h at −20 °C. Two different types of X-ray quality crystals formed. X-ray diffraction confirmed that one of the crystal products was Cp^*_2Co (deep violet) and the other was found to be the complex $[UO_2(salan\text{-}^tBu_2)(py)][Cp^*_2Co]$ (**6**) (orange). However, all of the attempts to separate the two compounds in a larger synthesis failed due to their similar solubility properties in pyridine. ^{1}H NMR (Pyridine-d_5; 298 K; 200 MHz): −12.81 (br, 2H); −10.17 (br, 2H); −7.08 (s, 3H, $-N(CH_3)-$); −6.18 (br, 2H, $-NCH_2-$Ph); −4.56 (s, 18H, $-^tBu$); 0.11 (s, 18H, $-^tBu$); 2.76 (s, 2H, $-CH-_{aromatic}$); 4.55 (s, 2H, $-CH-_{aromatic}$); 9.28 (br, 2H, $-NCH_2-$Ph).

The NMR spectrum of a solution of **5** in deuterated pyridine recorded after addition of 2 equiv of Cp^*_2Co still shows much broader signals than those found for $[UO_2(salan\text{-}^tBu_2)(py)\ K]_n$. The addition of $[UO_2(salan\text{-}^tBu_2)(py)]$ to this reaction mixture does not result in the presence of additional signals but only in the further broadening of the U(V) peaks and shift of the signals. These results point to the presence of U(VI) and U(V) exchanging species even in the presence of an excess of Cp^*_2Co and suggests that the two redox systems $Cp^*_2Co^+/Cp^*_2Co$ and UO_2^{2+}/UO_2^+ are in equilibrium in pyridine solution.

The addition of potassium iodide leads to the formation of **3**.

Dissolution of **6** in toluene results in its complete reoxidation to the hexavalent complex **5** due to the solvent influence on the redox potential and to the presence of the redox active counterion.

Synthesis of $[UO_2(salophen\text{-}^tBu_2)(py)K]$ (7). A solution of 69.0 mg of $K_2(salophen\text{-}^tBu_2)$ (0.112 mmol, 1 equiv) in pyridine (3.0 mL) was added to 124.9 mg (0.112 mmol) of $\{[UO_2py_5][KI_2py_2]\}_n$ resulting, within minutes, in a dark-green solution. The solution was evaporated under vacuum to the volume of 0.5 mL. The addition of $^iPr_2O$ (10 mL) to the resulting solution afforded a green solid that was filtered, washed 3 times with 4 mL $^iPr_2O$ and dried under vacuum. Yield: 95.0 mg (74%). ^{1}H NMR (Pyridine-d_5; 298 K; 400 MHz): −2.26 (s, 9H, $-^tBu$), 0.58 (s, 9H, $-^tBu$), 3.17 (br. 1H, -NPh-), 4.55 (s, 1H, $-CH\text{-}_{aromatic}$); 6.27 (br. 1H, -NPh-); 7.34 (s, 1H, $-CH\text{-}_{aromatic}$); 7.69 (s, 1H, $-CH{=}N-$). Anal. Calcd for $[UO_2(salophen\text{-}^tBu_2)(py)K]\cdot 1.33KI$ $C_{41}H_{51}UN_3O_4K_{2.33}I_{1.33}$: C, 42.86; H, 4.44; N, 3.66. Found: C, 42.86; H, 4.56; N, 3.57.

Crystals of complex $\{[UO_2(salophen\text{-}^tBu_2)(thf)]K(thf)_2\}_n$, **8** were obtained by recrystallization of complex **7** from thf solution (6.9 mM) over 3 days.

Synthesis of $[UO_2(salophen\text{-}^tBu_2)(py)]$ (9). A light yellow pyridine solution (2 mL) of $UO_2(NO_3)_3$, $5H_2O$ (66.9 mg, 0.124 mmol, 1eq.) was added to a pyridine solution (2 mL) of $H_2salophen\text{-}^tBu_2$ (49.4 mg, 0.124 mmol, 1eq.). The resulting red solution was stirred for 2 h at room temperature. The solvent was evaporated in *vacuum* (1 mL) and hexane was slowly layered on the top. After 16 h (overnight) at −18 °C a red powder formed and was filtrated to yield 38 mg (35%) of $[UO_2(salophen\text{-}tBu_2)(py)]$. ^{1}H NMR (Pyridine-$d_5$; 298 K; 400 MHz): 9.79 (s, 2H); 8.02 (d, 2H, $J = 9.6$ Hz); 7.83 (d, 2H, $J = 9.4$ Hz); 7.54 (m, 2H); 7.37 (m, 2H); 1.50 (s, 18H); 1.48 (s, 18H). UV: 432 nm ($\varepsilon = 17676\ cm^{-1}\ mol^{-1}$), 357 nm ($\varepsilon = 31703\ cm^{-1}\ mol^{-1}$). Anal. calcd for $C_{41}H_{51}O_4N_3U$: C, 55.46; H, 5.79; N, 4.73. Found: C, 55.46; H, 5.99; N, 5.19.)

Stability Studies. The stability of **3**, **4**, **6** and **7** was investigated in pyridine-d_5. For each sample, the concentration was about several mM (**4** − 4.72 mM, **7** − 6.90 mM, **3** − 7.24 mM) and the samples were monitored in time by ^{1}H NMR at 400 MHz and 298 K. The stability in presence of water was also studied by ^{1}H NMR at 400 MHz and 298K in 1:X (X, 1−1000) mixture of the complex and water in pyridine.

X-Ray Crystallography. Diffraction data were taken using a Oxford-Diffraction XCallibur S Kappa geometry diffractometer (Mo Kα radiation, graphite monochromator, $\lambda = 0.71073$ Å). To prevent evaporation of cocrystallized solvent molecules the crystals were coated with light hydrocarbon oil and the data were collected at 150 K. The cell parameters were obtained with intensities detected on three batches of 5 frames. The crystal-detector distance was 4.5 cm. For three settings of Φ and θ, 196 narrow data were collected for 1° increments in ω with a 20 s exposure time for **2**, 60 s for **4**, 120 s for **6** and 30 s for **8**. Unique intensities detected on all frames using the Oxford-diffraction Red program were used to refine the values of the

(60) Avens, L. R.; Bott, S. G.; Clark, D. L.; Sattelberger, A. P.; Watkin, J. G.; Zwick, B. D. *Inorg. Chem.* **1994**, *33*, 2248–2256.

Table 6. Crystallographic Data for Complexes, **4**, **6** and **8**

	4·2(Toluene)	**6**·4.5C_5H_5	**8**
Formula	C65 H99 K N3 O10 U	C81.50 H111.50 Co N7.5 O4 U	C52 H78 K N2 O8 U
Crystal size (mm)	0.1 × 0.1 × 0.05	0.15 × 0.04 × 0.03	0.34 × 0.12 × 0.07
cryst system	Monoclinic	Triclinic	Monoclinic
space group	*C*2/*c*	$P\bar{1}$	*P*21/*c*
volume (Å^3)	13297.5(4)	4044.7(11)	5223.89(9)
a (Å)	31.4372(6)	11.850(2)	17.46080(19)
b (Å)	20.4126(4)	13.9279(12)	21.55872(18)
c (Å)	20.8384(3)	26.375(5)	15.06929(15)
α (deg)	90	82.170(10)	90
β (deg)	96.0642(19)	84.019(14)	112.9413(12)
γ (deg)	90	69.999(12)	90
Z	8	2	4
formula weight (g/mol)	1359.60	1557.24	1136.29
density (calcd) (g cm^{-3})	1.358	1.279	1.445
absorption coefficient (mm^{-1})	2.559	2.255	3.239
F(000)	5608	1608	2316
temp (K)	150.(2)	150(2)	150(2)
total no. reflections	34513	15349	65088
unique reflections	13293 [0.0286]	9270 [0.0605]	12734 [0.0299]
Final *R* indices [$I > 2\sigma(I)$]	$R1 = 0.0320$, $wR2 = 0.0695$	$R1 = 0.0756$, $wR2 = 0.1745$	$R1 = 0.0257$, $wR2 = 0.0532$
Largest diff. peak and hole (e.A^{-3})	2.440 and −0.534	4.440 and −0.932	1.172 and −0.529
GOF	0.919	1.003	0.882

cell parameters. The substantial redundancy in data allows empirical absorption corrections to be applied using multiple measurements of equivalent reflections with the ABSPACK Oxford-diffraction program. Space groups were determined from systematic absences, and they were confirmed by the successful solution of the structure (Table 6). The structures were solved by direct methods using the SHELXTL 6.14 package and for all structures all atoms, including hydrogen atoms, were found by difference Fourier syntheses. All non-hydrogen atoms were anisotropically refined on *F* in **2** and **6** and **8**. For **4** disordered tert-butyl C29b, C30b and C31b (occupancy factor at 0.13) has been refined isotropically. For **2** and **6,** hydrogen atoms were fixed in ideal position. For **4**, hydrogen atoms were refined isotropically except for toluene solvents and disordered tert-butyl for which the hydrogen atoms have been constrained. For **8**, Hydrogen atoms were refined isotropically except for three thf molecules and the disordered tert-butyl for which the hydrogen atoms have been constrained.

Acknowledgment. This work was supported by the Commissariat à l'Energie Atomique, Direction de l'Energie Nucléaire. We thank Pierre Alain Bayle for his help with the NMR experiments and Jean-François Jacquot for the magnetic measurements.

Supporting Information Available: Crystallographic details for compounds **4**, **6** and **8** (as CIF files), UV−visible spectra of **1**, **2**, **4**, **6**−**7** and **9**, NMR spectra and IR spectra of **4**, **5**, **7** and **9**, electrochemistry data for compounds **3**−**5** and **7**−**9**, EPR data for **4** and experimental description of the reactivity with water. Computational data. This material is available free of charge via the Internet at http://pubs.acs.org.

JA9037164

(61) Enriquez, A. E.; Scott, B. L.; Neu, M. P. *Inorg. Chem.* **2005**, *44*, 7403–7413.